Energy Storage Materials 55 (2023) 538–545

Contents lists available at ScienceDirect

Energy Storage Materials

journal homepage: www.elsevier.com/locate/ensm

A novel hydrophobic-zincophilic bifunctional layer for stable Zn metal anodes

Xuan Zhou [a,1], Renpeng Chen [a,1], Enhui Cui [a], Qin Liu [a], Hong Zhang [a], Jiahui Deng [a], Nannan Zhang [a], Can Xie [a], Lin Xu [a,b,c,*], Liqiang Mai [a,b,c]

[a] State Key Laboratory of Advanced Technology for Materials Synthesis and Processing, School of Materials Science and Engineering, Wuhan University of Technology, Wuhan 430070, Hubei, China
[b] Hubei Longzhong Laboratory, Wuhan University of Technology (Xiangyang Demonstration Zone), Xiangyang 441000, Hubei, China
[c] Hainan Institute, Wuhan University of Technology, Sanya 572000, China

ARTICLE INFO

Keywords:
Bifunctional layer
Anti-corrosion
Uniform deposition
Surface modification
Zn metal anode

ABSTRACT

Zn metal serving as anode endows aqueous Zn-ion batteries (AZBs) attractive advantages of high energy density, inherent safety and low cost. However, direct contact between electrolytes and Zn metal leads to severe surface corrosion and dendrite growth, which have greatly compromised the calendar life and Coulombic efficiency (CE) of AZBs. Herein, a novel hydrophobic-zincophilic bifunctional layer (HZBL) is introduced on Zn surface (HZBL-Zn) to provide hydrophobic and uniform pathways for zinc ions. In this unique design, hydrophobic framework serves as a buffer layer to isolate active Zn from bulk electrolytes, and meanwhile zincophilic functional groups on sidechains form uniform pathways to regulate Zn deposition behavior. Correspondingly, HZBL can not only inhibit notorious side reaction but promote the uniform deposition on Zn surface. With this synergy effect, HZBL-Zn symmetrical cells stably perform 2500 h with 40 mV polarization voltage at 1 mA cm^{-2} with a capacity of 1 mAh cm^{-2}. Surprisingly, the average CE of Zn stripping/plating underneath HZBL reach 99.88% after 2700 cycles. This concept of hydrophobic-zincophilic bifunctional molecular reassembly holds great prospects in the development of highly stable Zn metal anodes.

Introduction

Considering the increasing focus on safety, those rechargeable batteries with aqueous electrolytes usher in an opportunity for their renaissance [1,2], among which aqueous Zn-ion batteries (AZBs) are highly preferred to be next generation electronics owing to the high resource abundance, low reduction potential (versus standard hydrogen electrode, -0.762V) and high theoretical specific capacity (820 mAh g^{-1} and 5855 mAh cm^{-3}) of Zn metal [3,4]. However, as the most common anode, Zn metal tremendously hampers the further development of AZBs due to its intrinsic drawbacks: both thermodynamic and electrochemical instability in conventional aqueous electrolyte, which are manifested as surface corrosion and dendrite growth [5,6]. These problems are mainly related to the direct contact of electrolytes and Zn metal surface [7]. Generally in aqueous electrolytes, zinc ion exists in a solvated structure formed with six water molecules [8]. The desolvation process must be achieved to release free zinc ions for the further deposition behavior in the inner Helmholtz plane (IHP) when solvated zinc ions pass through the Helmholtz plane (HP) from the diffusion layer [9]. However, because of the rising overpotential caused by strong interaction, water molecules that form solvated shells with zinc ions are more inclined to be reduced to H_2 on the surface of Zn anodes [10]. Afterwards, the local increased OH^- induced by hydrogen evolution reaction (HER) will combine with zinc ions to form insulating by-products (e.g., $Zn_4(OH)_6SO_4{\cdot}xH_2O$), which consumes excess electrolytes and reduces the Coulombic efficiency (CE) of limited Zn metal [11]. Unlike the desirable dense solid electrolyte interphase (SEI) film in LIBs, the by-products from HER in AZBs are too loose to prevent inner Zn metal from further corrosion [12]. As depicted in Fig. 1a, bare Zn surface inevitably undergoes HER induced by water and followed by the formation of by-products. And in the case of electrification, zinc ions prefer to nucleate and grow on lumped sites rather than their nearby areas to form protuberances since the lower surface energy and higher migration energy [13,14]. The already formed protuberances will provide more

* Corresponding author.
E-mail address: linxu@whut.edu.cn (L. Xu).
[1] These authors contributed equally to this work.

https://doi.org/10.1016/j.ensm.2022.12.019
Received 22 August 2022; Received in revised form 1 December 2022; Accepted 12 December 2022
Available online 14 December 2022

active sites for the deposition of zinc ions as a result of so-called "tip effect", and promote the formation of dendrites in the form of positive feedback. After conductive dendrites pierce the separator and connect both electrodes of the battery, it will lead the battery to fail [15,16].

Up to now, great efforts have been paid to address the obsession of notorious corrosion and dendrite growth in AZBs. A conventional method of designing conductive hosts with increased specific surface area, including 3D Cu [17,18], Zn/CNTs foam [19,20], MOF-derived Zn [21,22] and so on [23,24], can alleviate polarization and provide more sites for deposition. In addition, exploiting new electrolytes with reduced water activity to ameliorate HER has aroused wide interest, such as preparing high concentration electrolytes [25,26], adopting nonaqueous electrolytes [27,28] and adding electrolyte additives [29,30]. Among those methods, surface coating is a more direct one to separate Zn anodes from electrolytes and less constrained by the availability of electrodes and electrolytes. Recently, various attractive strategies about coating layers on Zn surface have been reported to solve the corrosion and dendrite issues, such as gel-based layer [31,32], elastic interface [33] and hydrophobic supramolecular network [34], which are proved to be truly effective. As a scalable strategy with simple preparation process, introducing coating layer onto the surface of Zn anodes is a potential candidate, which include inorganic, organic, and hybrid ones [35–38]. However, the inorganic coating layers tend to crush or fall off when the Zn surface undergoes volume expansion due to continuous plating/stripping behavior [39]. Meanwhile, the poor dispersibility of inorganic particles in organic systems greatly compromises the expected function of the hybrid protective layers [38]. In comparison, organic coatings with good mechanical properties can be uniformly dispersed and accommodate continuous volume change during charging and discharging. Among those organic layers, a hydrophobic monofunctional one causes an increased surface polarization which is not conducive to Zn deposition. Similarly, an excessively hydrophilic organic layer with zincophilic groups that can promote the uniform deposition of zinc ions dissolves easily in aqueous electrolytes, unable to protect Zn anodes. Since corrosion and dendrites are symbiotic issues that need to be simultaneously addressed, the adverse effect of hydrophobicity of organic coating layers should be properly solved.

Herein, we design a novel hydrophobic-zincophilic bifunctional layer (HZBL) that can not only inhibit surface corrosion but induce the uniform Zn deposition. The HZBL artificial layer, synthesized by free radical polymerization of polyvinylidene fluoride (PVDF) and acrylic acid, is coated on the surface of Zn anodes (HZBL-Zn). It is clear in Fig. 1b that HZBL can not only effectively inhibit the corrosion, but precisely control the deposition of zinc ions. That is because, on the one hand, the hydrophobic framework is favorable for isolating active water; on the other hand, zincophilic −COOH groups will provide uniform transport pathways for zinc ions through the strong adsorption (Fig. 1c), which is confirmed by density functional theory (DFT) calculations. Moreover, the desolvation energy is significantly reduced, which favors the deposition kinetics of zinc ions for higher rate performance and longer cycle life [40]. Correspondingly, HZBL enables symmetrical cells to stably perform 2500 h with 40 mV polarization voltage at 1 mA cm^{-2},

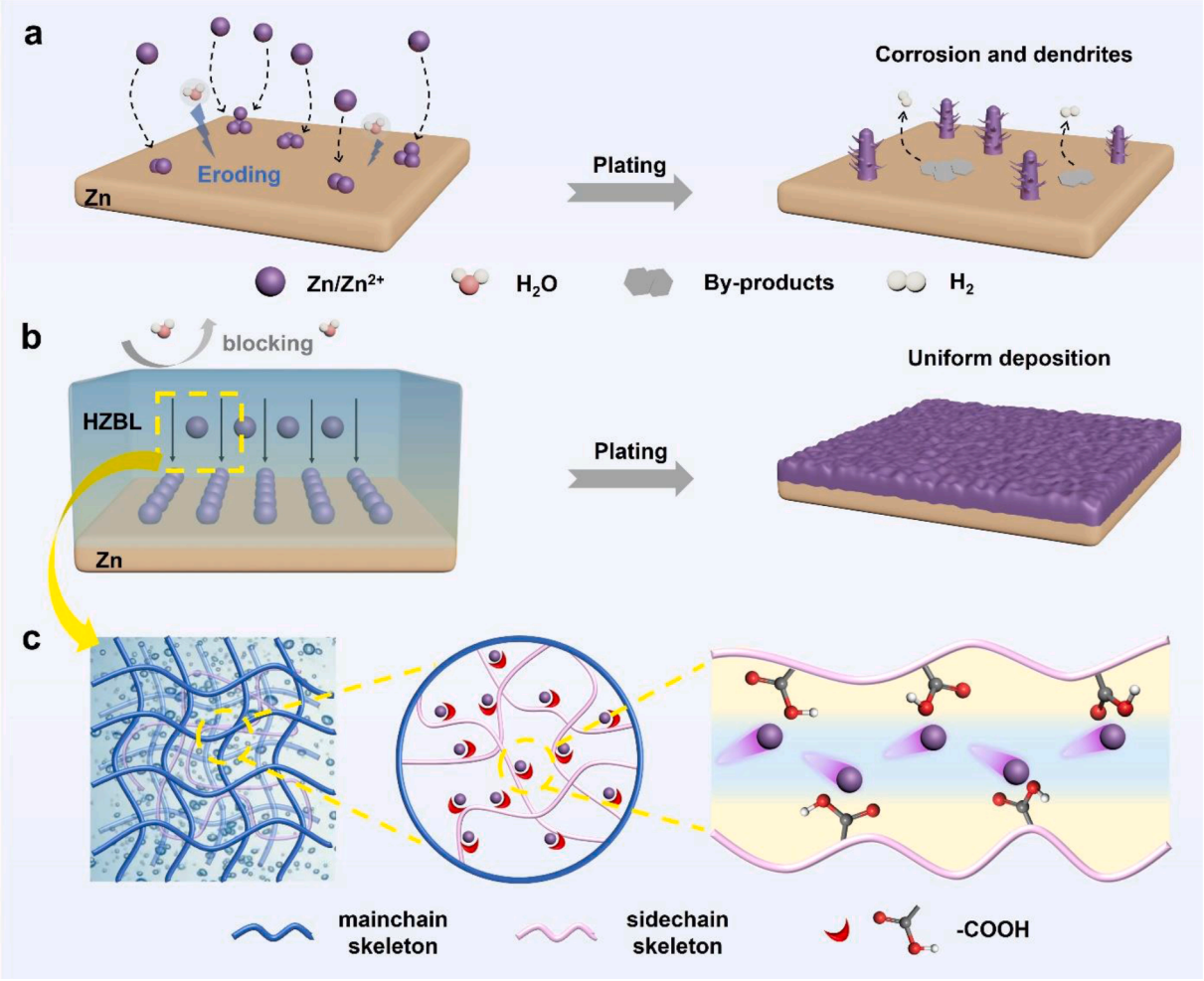

Fig. 1. Schematic diagrams of corrosion situation and Zn plating behavior during charge process on the anodes of a) bare Zn and b) HZBL-Zn. c) Gradually enlarged schematic of the uniform transport pathways of zinc ions in HZBL.

greatly prolonging the cycle life of Zn anodes. Moreover, the average Coulombic efficiency (CE) of Zn stripping/plating underneath the HZBL reach 99.88% after 2700 cycles, 15 times longer than bare Zn. When assembled with MnO_2, HZBL-Zn full cell delivers a stinkingly enhanced capacity retention which is higher than that of bare Zn full cell. This simple and low-cost but effective strategy designates a new way for the development of Zn anodes.

Results and Discussion

Fig. 2a depicts the structure diagram of the repeating units of HZBL. This target product was obtained by first dissolving PVDF in 2 M KOH/ethanol solution to generate C=C bonds, and followed by free radical polymerization to grow branches in N-Methylpyrrolidone (NMP). In order to confirm the successful preparation of HZBL, a series of characterizations were carried out. As shown in X-ray photoelectron spectroscopy (XPS) results, the characteristic peaks of C−O and C=O can be observed in both C 1s (Fig. 1b) and O 1s (Fig. 1c) spectra of HZBL [41,42]. The appearance of C−F in C 1s spectrum is consistent with that in F 1s spectrum (Fig. S1) [43]. Then, in Fourier transform infrared spectrometer (FTIR) (Fig. 2d) spectrum, the characteristic peaks of 3428 cm^{-1} and 1620 cm^{-1} are attributed to the emerging of O−H. And the absorption peaks located at 1723 cm^{-1}, 840 cm^{-1} and 510 cm^{-1} are related to the existence of C=O (vibrating), CH_2 (rocking) and CF_2 (bending), respectively [44,45]. The flow diagram about the preparation of HZBL-Zn is shown in Fig. S2. During this progress, HZBL was first evenly dissolved in NMP with constant stirring for 7 days to produce sample solution. Then, the as-prepared solution was tiled on the surface of Zn anode by spin coating method. The successful preparation of HZBL-Zn was also proved. According to the scanning electron microscopy (SEM) images, HZBL-Zn (Fig. 2e) delivers a much smoother and flatter surface than bare Zn (Fig. S3). And around 15 μm coating thickness in this work (Fig. 2f) is much thinner than that of the reported one [46]. Importantly, the close contact of HZBL and Zn anode can be clearly seen from the element mapping images (Fig. 2g), with uniform distribution of C, O, F elements on Zn. This is mainly ascribed to the strong adhesion of oxygen-containing functional groups to Zn metal.

In order to testify the improved anti-corrosion properties of the Zn anodes with designed layer, bare Zn, HZBL-Zn were soaked in 2 M $ZnSO_4$ electrolyte for 14 days. As shown in Fig. S4, the optical photos of two initial Zn foils all present their metallic luster. However, after being soaked and drying in the air, the surface flatness of them differs significantly. Apparently, a large number white blocks are observed on bare Zn after being soaked for 14 days compared to much cleaner and flatter surface of HZBL-Zn, which is consistent with SEM results (Fig. S5). The different surface conditions of the as-two foils after long-time immersion disclose that HZBL can prevent Zn surface from direct contact with electrolytes to inhibit corrosion. Further, taffel test was conducted to prove the positive effect of HZBL on interfacial corrosion of Zn anode in 2 M $ZnSO_4$ solution (Fig. S6). It is obvious that HZBL-Zn exhibits an increased corrosion potential from -1.09 V to -1.06 V and a decreased corrosion current from 2.27 mA cm^{-2} to 0.79 mA cm^{-2} compared to bare Zn. These changes demonstrate that with HZBL, Zn anode delivers a lower tendency to be corroded and a lower corrosion rate [47]. Meanwhile, the effect of the modified layer on HER can also be verified by linear polarization curves (Figure S7). HZBL-Zn shows higher overpotential of HER than that of bare Zn, further reflecting that the HZBL can suppress HER on Zn surface.

Besides corrosion suppression, it is also essential for artificial layer to regulate the transmission and growth behavior of Zn to avoid dendrites. PVDF was coated on Zn foil (denoted as PVDF-Zn) as control sample to highlight the superiority of our HZBL on restricting Zn uniform deposition. Symmetrical Zn cells were assembled in a transparent tank to obtain Zn-deposited anodes. Apparently in digital photos, HZBL-Zn delivers a uniform surface appearance after Zn plating, while Zn is unevenly and randomly deposited on bare Zn and PVDF-Zn (Fig. S8). This sharp difference can also be identified in their cross-sectional SEM images (Fig. 3a,b and Fig. S9). It is obvious in Fig. 3b that deposited Zn is uniformly distributed under the intact HZBL, which is consistent with its plane SEM image in Fig. S10, meanwhile indicating the strong

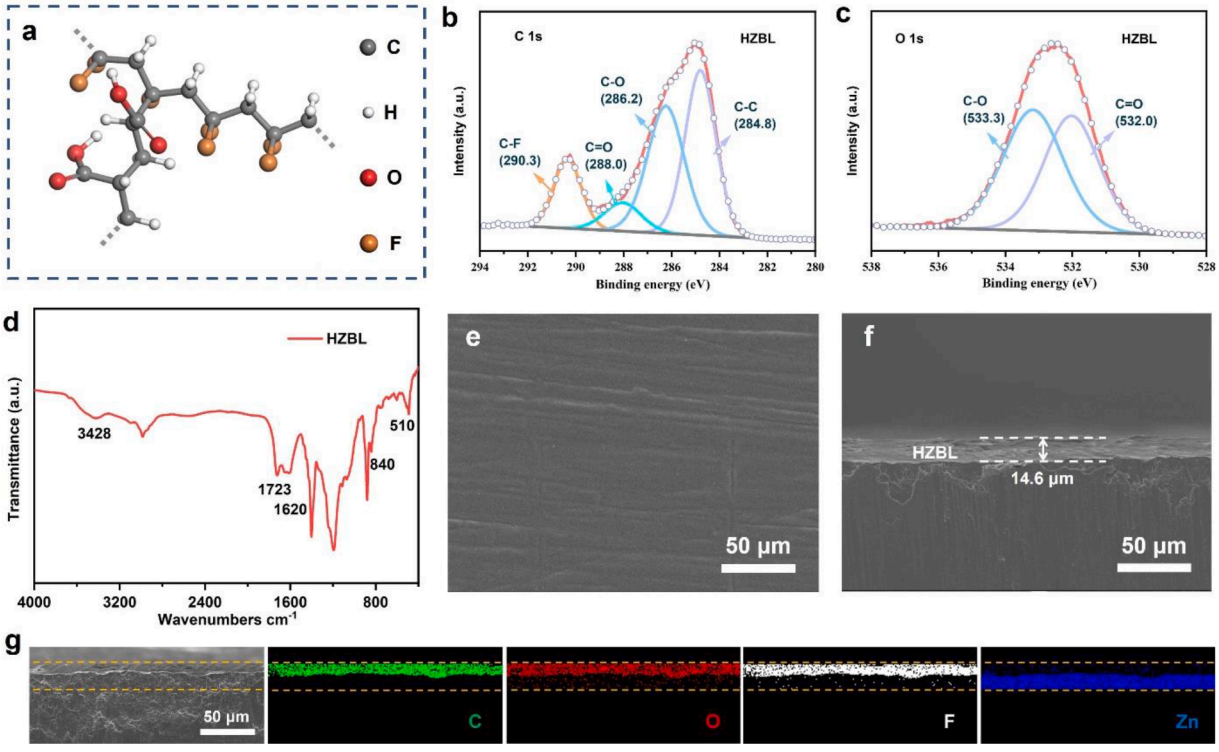

Fig. 2. Designed synthesis and characterizations of HZBL-Zn. a) The structure diagram of repeating units of HZBL. b, c) XPS C 1s and O 1s spectrum of HZBL, respectively. d) FTIR spectrum of HZBL. e) Plane and f) cross-sectional SEM images of initial HZBL-Zn. g) Element mapping images of cross-section for HZBL-Zn.

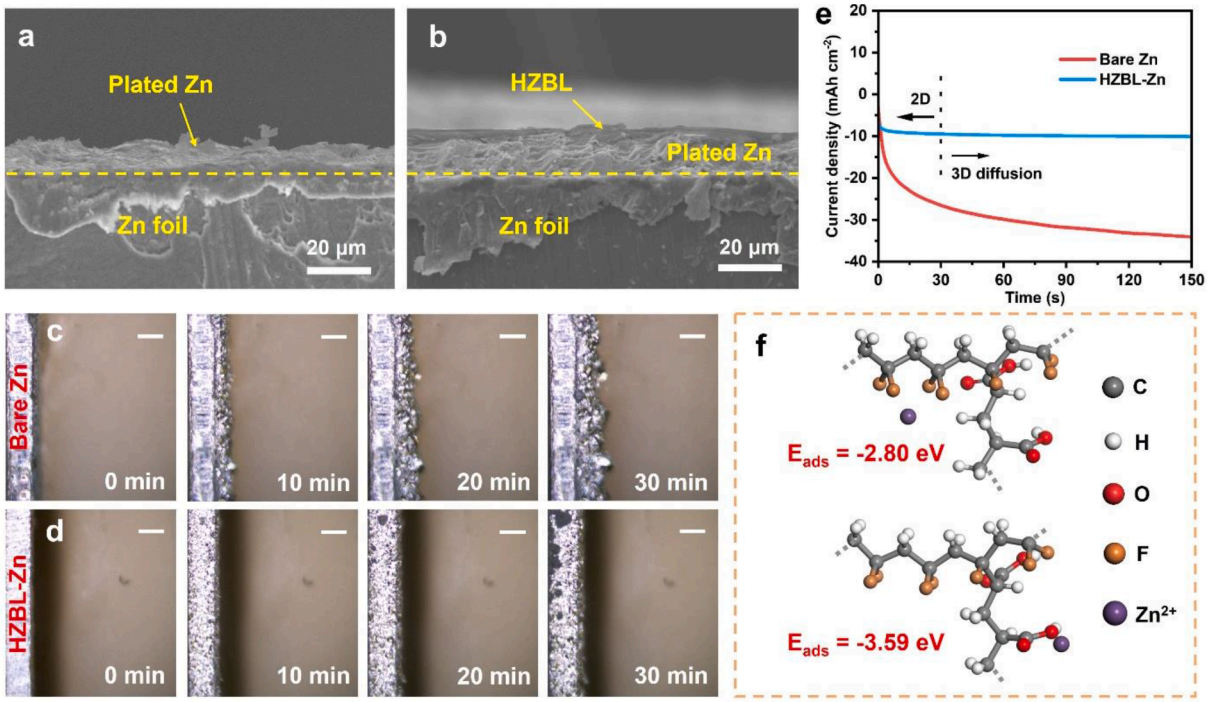

Fig. 3. Characterizations of Zn plating behavior on HZBL-Zn. Cross-sectional SEM images of a) bare Zn and b) HZBL-Zn after continuous Zn plating/stripping at a current density of 2 mA cm^{-2} in transparent symmetrical cells for 1 h. In situ optical microscope results of c) bare Zn and d) HZBL-Zn at the current density of 10 mA cm^{-2}. Scale bar: 200 μm. e) CAs of bare Zn and HZBL-Zn at a -150 mV overpotential. f) DFT calculation results for adsorption energy of zinc ion with −F groups and −COOH groups on HZBL.

mechanical properties of this artificial layer. Then, we used a four-point probe tester (HPS2661) to test the resistance value of HZBL membrane. According to the result, the resistivity of HZBL membrane is beyond the range of 2 MΩ cm^{-1}, which can be considered electrical insulation. Thus, when HZBL is coated on Zn surface, plated Zn will grow under HZBL layer. To visually evaluate the influence of HZBL on uniform deposition, an in-situ observation was conducted under an optical microscopy. That is to monitor the evolution of the Zn-electrode surface morphology under 10 mA cm^{-2} for 30 min. As Fig. 3c shows, the Zn deposition on bare Zn surface has been already nonuniform with messy protuberances within the first 10 minutes. And gradually, spiny dendrites appear over time since zinc ions prefer to deposit on existing protrusions. If these dendrites continue to grow, they will pierce the glass fiber to connect the electrodes, resulting in short circuit of the battery, which causes great trouble to its application. In Fig. S11, although sharp dendrites like those on the surface of bare Zn cannot be seen on PVDF-Zn surface, it is obvious that the nucleation of Zn remained uneven. This is mainly due to the increased surface polarization caused by the hydrophobicity of PVDF. In sharp contrast, HZBL-Zn surface keeps flat and smooth during the whole plating process and almost no protrusions form, indicating that HZBL can restrain the deposition of zinc ions (Fig. 3d).

Additionally, chronoamperometry (CA) test was conducted to examine the intrinsic mechanism of Zn nucleation and growth. That is to apply an overpotential of −150 mV on symmetric cells and record current-time profiles. As shown in Fig. 3e, the current of bare Zn continues to increase during the whole process while that of HZBL-Zn reaches 9.7 mA cm^{-2} within 30 s and remains stable for the rest of the time. In fact, an increased current indicates a 2D diffusion process where zinc ions are inclined to aggregate and form dendrites to minimize specific surface area and surface energy [48]. And a stable current indicates a 3D state, which is ascribed to an additional energy barrier provided by HZBL to force zinc ions to nucleate in very close sites and facilitate uniform growth [49]. This energy barrier is derived from the strong adsorption of zinc ion with zincophilic −COOH group on HZBL, which is confirmed by DFT calculation results. As shown in Fig. 3f and Fig. S12, the adsorption energy of zinc ion with −F group on PVDF (-2.66 eV) and −F group on HZBL (-2.80 eV) is lower than the binding energy of zinc ion with water molecule (-3.08 eV), while the adsorption energy of zinc ion with zincophilic −COOH group on HZBL (-3.59 eV) is the highest. The comparison result demonstrates that zinc ions are prone to combine with −COOH groups on HZBL and -F groups cannot realize Zn uniform plating. So that under the effect of electric field, zincophilic −COOH groups in HZBL will form uniform pathways with multiple transfer sites for zinc ions, thus restraining the process of their deposition.

Since solvated zinc ions must be released to be free ions when they pass through HP from diffusion layer to perform plating behavior in IHP, the desolvation process is crucial to the stability of Zn anodes. The EIS measurements of bare Zn, PVDF-Zn and HZBL-Zn symmetric cells at different temperatures were conducted to obtain their activation energy during Zn deposition (Fig. S13). HZBL-Zn cell delivers lower charge-transfer resistance than the other two cells under different temperatures. According to the Arrhenius equation [50], the activation energy of HZBL-Zn is calculated as 26.02 kJ mol^{-1}, much lower than 30.66 kJ mol^{-1} of PVDF-Zn and 31.15 kJ mol^{-1} of bare Zn (Fig. S14). The decreased activation energy of HZBL-Zn indicats that HZBL could promote the transfer rate and desolvation process of zinc ions, which was confirmed by DFT results of the desolvation energy on different Zn anodes. As depicted in Fig. 4a, each zinc ion will form a solvated structure with six water molecules, which delivers a high desolvation energy of -9.72 eV. Meanwhile, without protection, the removed active water molecules will directly contact with Zn metal surface to induce corrosion. However, the desolvation energy of zinc ion is reduced to -6.79 eV with the protection of our designed HZBL (Fig. 4b), which greatly improve the kinetics of Zn plating/stripping and ensure uniform deposition. Importantly, due to the hydrophobic skeleton of HZBL, the removed water molecules will be isolated from metal surface, thus preventing corrosion and realizing highly stable Zn metal anodes.

The cycling reversibility and stability in a long-term electrochemical environment is an important basis for evaluating the quality of Zn

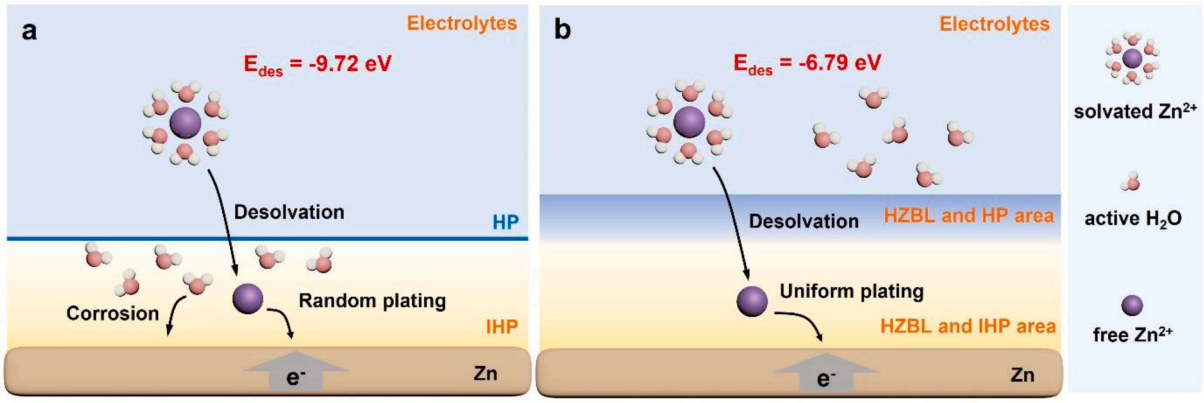

Fig. 4. Mechanism of the transmission and deposition process of zinc ions. Schematic diagrams of the desolvation and deposition process of zinc ions on a) bare Zn and b) HZBL-Zn.

anodes. As shown in Fig. 5a, HZBL-Zn symmetric cells display much longer lifespan of 2500 h at 1 mA cm^{-2}/1 mAh cm^{-2} than PVDF-Zn (350 h) and bare Zn (190 h) cells. It is obvious in the inserts that HZBL-Zn leads cells to a smaller and more stable polarization voltage (around 40 mV), which is mainly because HZBL can promote the desolvation process of zinc ions and accelerate ion transport. Surprisingly, such a long lifespan is superior to most of the reported Zn anodes with other different coating layers (Table S1). Then, X-ray diffraction (XRD) was conducted to analyze the different corrosion conditions between bare Zn and HZBL-Zn surface after 100 cycles (200 h). In Fig. 5c, cycled HZBL-Zn

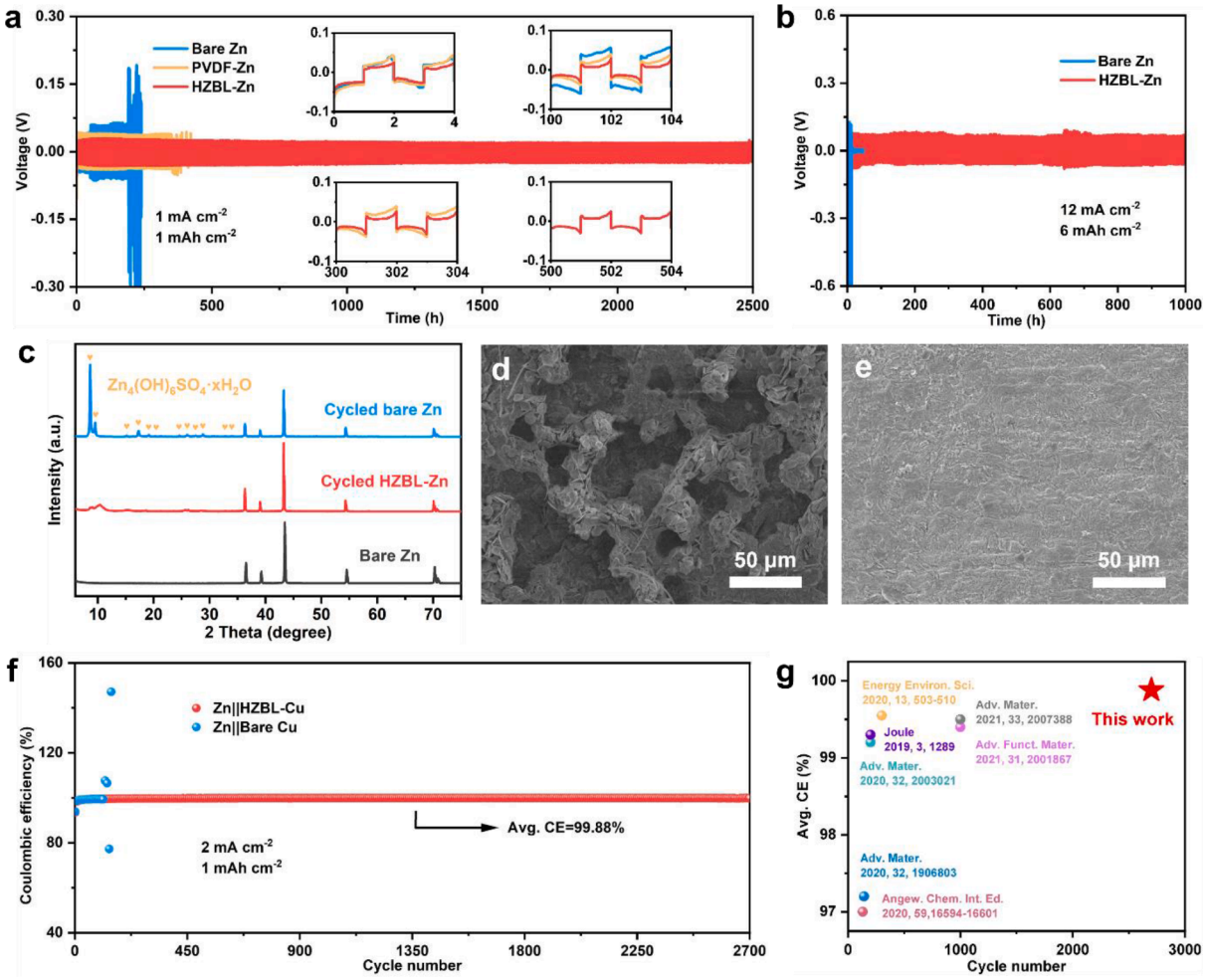

Fig. 5. Reversibility of Zn plating/stripping behavior in different symmetric cells. a) Long-term cycling performance of bare Zn||bare Zn, PVDF-Zn||PVDF-Zn and HZBL-Zn||HZBL-Zn at constant current density of 1 mA cm^{-2} with the inset showing partial enlarged profiles of them. b) Voltage-time profiles of Zn symmetric cells with bare Zn and HZBL-Zn at 12 mA cm^{-2}, 6 mAh cm^{-2}. c) XRD patterns of bare Zn and HZBL-Zn and corresponding SEM images of d) bare Zn and e) HZBL-Zn after cycling for 200 h at current density of 1 mA cm^{-2}. f) CE of long-term cycles in Zn||bare Cu and Zn||HZBL-Cu at a current density of 2 mA cm^{-2}. g) Comparison between this work and others about CE and cycle number.

delivers much weaker peaks of by-products $Zn_4(OH)_6SO_4{\cdot}xH_2O$ compared to cycled bare Zn, which suggests the important role of HZBL in terms of anti-corrosion. Correspondingly, many irregular protrusions and fibrous substances are observed on the surface of cycled bare Zn after (Fig. 5d), which indicates that dendrites might have punctured the separator. However, cycled HZBL-Zn remained flat and clean, with few dendrites on it (Fig. 5e). Even as the current density and areal capacity are increased to 12 mA cm^{-2} and 6 mAh cm^{-2} in Fig. 5b, HZBL-Zn cells can circulate stably for 1000 h with polarization voltage of 160 mV, proving the enhanced ability of HZBL to inhibit dendrite growth and corrosion on the surface of Zn anodes. In sharp contrast, bare Zn cell is unbearable to this high current density and failed after several cycles. The rapid failure of bare Zn cells should be attributed to drastic dendrite growth and unstoppable electrolyte corrosion at the solid-liquid interface (Fig. S15). The increased overpotential from 40 mV of 1 mA cm^{-2} to 160 mV of 12 mA cm^{-2} should be attributed to the positive relativity of overpotential with current rate, and the shorter cycle time of cells under 12 mA cm^{-2} is due to the decreased Sand's time [51].

Further, the improved rate performance of coated Zn anodes was also proved. With current density increased from 0.2 to 10 mA cm^{-2}, HZBL-Zn cells display almost no obvious fluctuation in the voltage range compared to bare Zn cell that is more sensitive to current changes (Fig. S16). The conductivity of zinc ions was determined by EIS test (Fig. S17). Calculation and analysis show that the ionic conductivity of HZBL is 1.17 mS cm^{-1}, much higher than that of PVDF layer (0.59 mS cm^{-1}). The enhanced ionic conductivity of HZBL should be ascribed to the zincophilic groups favoring the migration of zinc ions. The excellent rate performance of HZBL-Zn cells should be ascribed to enhanced transfer rate of zinc ions at the solid-liquid interface, which is consistent with the enhanced hydrophilicity. The dynamic contact angle test was conducted to confirm the enhanced hydrophilicity of HZBL-Zn at room temperature, and the results were illustrated in Fig. S18. Due to the intrinsic hydrophobicity of PVDF, the initial contact angle of PVDF-Zn is the largest initially and delivers the minimize decrease after 20 min. However, the contact angle of HZBL-Zn is smaller than bare Zn. From the perspective of thermodynamics, zinc ions display faster transfer rate and more uniform deposition on HZBL-Zn surface where the interfacial free energy between electrode and electrolyte is reduced because of the enhanced hydrophilicity [52]. Meanwhile, the electrochemical impedance spectroscopy (EIS) of symmetric cells was measured after different cycles. As shown in Fig. S19, the impedance of bare Zn cells delivers an intense fluctuation and is always greater than that of HZBL-Zn. The reason of this difference in stability might be attributed to the fewer by-products and dendrites on HZBL-Zn.

The Zn||Cu cells were constructed to further explore the CE (defined as the amount of plating/stripping) of limited Zn in enclosed environment, which is also crucial to the lifespan of anodes. PVDF and designed HZBL were coated on Cu foils by the same preparation method as HZBL-Zn (denoted as PVDF-Cu and HZBL-Cu, respectively). The mechanism of this test is that 1 mAh cm^{-2} of zinc ions is first dissolved from Zn metal anodes and deposited on the working electrode Cu while discharging, and then check how many zinc ions can be peeled off from the Cu during charging. As apparently shown in Fig. 5f, the CE of bare Cu fluctuates drastically at 180 cycles, even reaching 150%, indicating the short-circuiting of battery. Because of the intrinsic hydrophobicity, PVDF-Cu cells failed at the 170th cycle with an average CE of 99.42% (Fig. S20). In sharp contrast, HZBL-Cu cells display incredible stability for 2700 cycles (15 times longer than that of bare Cu cells) with the average CE of 99.88%. Fig. 5g represents the ultra-long cycle number and ultra-high average CE of HZBL-Cu when compared with other excellent works, proving its rationality and feasibility. Moreover, the enhanced cyclability and reversibility of coated Cu can also be confirmed by comparing the variation of polarization voltages between bare Cu cell and HZBL-Cu cell. In Fig. S21, the polarization voltage of bare Cu cell at the first cycle is 46.7 mV and it increases to 65.3 mV just after 100 cycles. Such a large change demonstrates that the plating and stripping of zinc ions without constraint is unstable. However, even after 2500 cycles, the polarization voltage of HZBL-Cu cell is still smaller than that of bare Cu cell, with a negligible change of 7 mV. This great superiority of HZBL-Cu in stability should give credit to the hydrophobic and uniform pathways for zinc ions. The SEM images of bare Cu and HZBL-Cu after 150 cycles are shown in Fig. S22. It can be seen that a large number of irregular block crystals are randomly covered on the surface of bare Cu and even pierced into the separator, which caused the crash of cells. By contrast, HZBL-Cu remains clean and smooth without pores or cracks. Meanwhile, the lower voltage hysteresis and nucleation overpotential of HZBL-Cu cells (Fig. S23) demonstrate that more sites for the deposition of zinc ions could be provided, thereby in a manner promoting the uniform deposition.

The contribution of HZBL-Zn to AZBs in full cells was further estimated by assembling with MnO_2 as cathodes. Traditional hydrothermal method was adopted to synthesize the cathode material MnO_2, whose morphology and purity were affirmed by SEM and XRD (Fig. S24 and Fig. S25), respectively. In order to prevent the disproportionation reaction of MnO_2 from affecting the evaluation of anode materials, 0.2 M $MnSO_4$ serving as additive was mixed with 2 M $ZnSO_4$. The stark contrast of the long-term cycling property between cells with bare Zn and HZBL-Zn is depicted in Fig. 6a. When tested at the current density of 3 C (C = 308 mA g^{-1}) and voltage range of 0.9-1.8 V, HZBL-Zn||MnO_2 presents an initial discharge specific capacity of 206.7 mAh g^{-1}, slightly higher than that of bare Zn||MnO_2 (198.9 mAh g^{-1}), and remains 166.1 mAh g^{-1} after 900 cycles with a high retention of 80.4%. Not surprisingly, the capacity of bare Zn||MnO_2 decays to 99.3 mAh g^{-1}, with a much lower retention of only 49.9%. As can be seen, the CEs of both the as-mentioned two full cells are above 99%. The better cycling performance of HZBL-Zn full cells should be ascribed to the ability of coating layer to inhibit side reaction and Zn dendrites, which is confirmed by the smooth surface of cycled HZBL-Zn (Fig. S26). It is apparent in Fig. 6b that the galvanostatic charge/discharge (GCD) curves of cells with bare Zn and HZBL-Zn have the similar characteristic platforms except for the higher capacity of the latter, which are in line well with their cyclic voltammogram (CV) results (Fig. 6c). As expected, there are two pairs of oxidation/reduction peaks in CV curves that represent the insertion/extraction reactions of zinc ions or hydrogen ions. Further, it can be inferred from Fig. 6d that HZBL-Zn full cell exhibits much better rate performance compared with bare Zn full cell. Both cells were examined under the current density from 1 C to 10 C. Despite the capacity of the bare Zn full cell (263.7 mAh g^{-1}) and HZBL-Zn full cell (266.7 mAh g^{-1}) are similar at first cycle, the latter can remain 106.8 mAh g^{-1} at 10 C and rise back to 251.6 mAh g^{-1} at 1 C, superior to the former. Even with limited Zn sources, HZBL-Zn full cells delivered a high capacity of 1.47 mAh initially and remained 0.7 mAh after 100 cycles (Fig. S27). Conversely, bare Zn full cells displayed an initial capacity of 1.36 mAh and decayed rapidly within 35 cycles and failed at around the 70^{th} cycle. The better performance of HZBL-Zn in the case of limited Zn source should be ascribed to the high reversibility of Zn platting/stripping under HZBL. Moreover, another reason of HZBL-Zn to improve the performance of its full battery—the designed layer can facilitate ion transmission, is indicated by the results of EIS (Fig. 6e).

In order to further prove the practical application of HZBL-Zn, it was packaged with MnO_2 into punch cells. As shown in Fig. 6f, the punch cell with HZBL-Zn delivered a stable open circuit voltage (OCV) of 1.417V. When a couple of the as-mentioned punch cells were in series and served as power supply, multiple light-emitting diodes (LEDs) could be successfully lighted up (Fig. 6g). Surprisingly, the OCV of the punch cell presented almost no or a little decrease after being folded and cut, demonstrating its intrinsic flexibility and safety (Fig. 6h,i). As shown in Fig. S28, the HZBL-Zn pouch cell keeps stable for 130 cycles and displays a high capacity retention of 85.9% (compared to the highest specific capacity of 205.1 mAh g^{-1}). The truth can be concluded from these test that the unique design in this work can not only solve the corrosion and dendrite-growth issues but adapt to practical application.

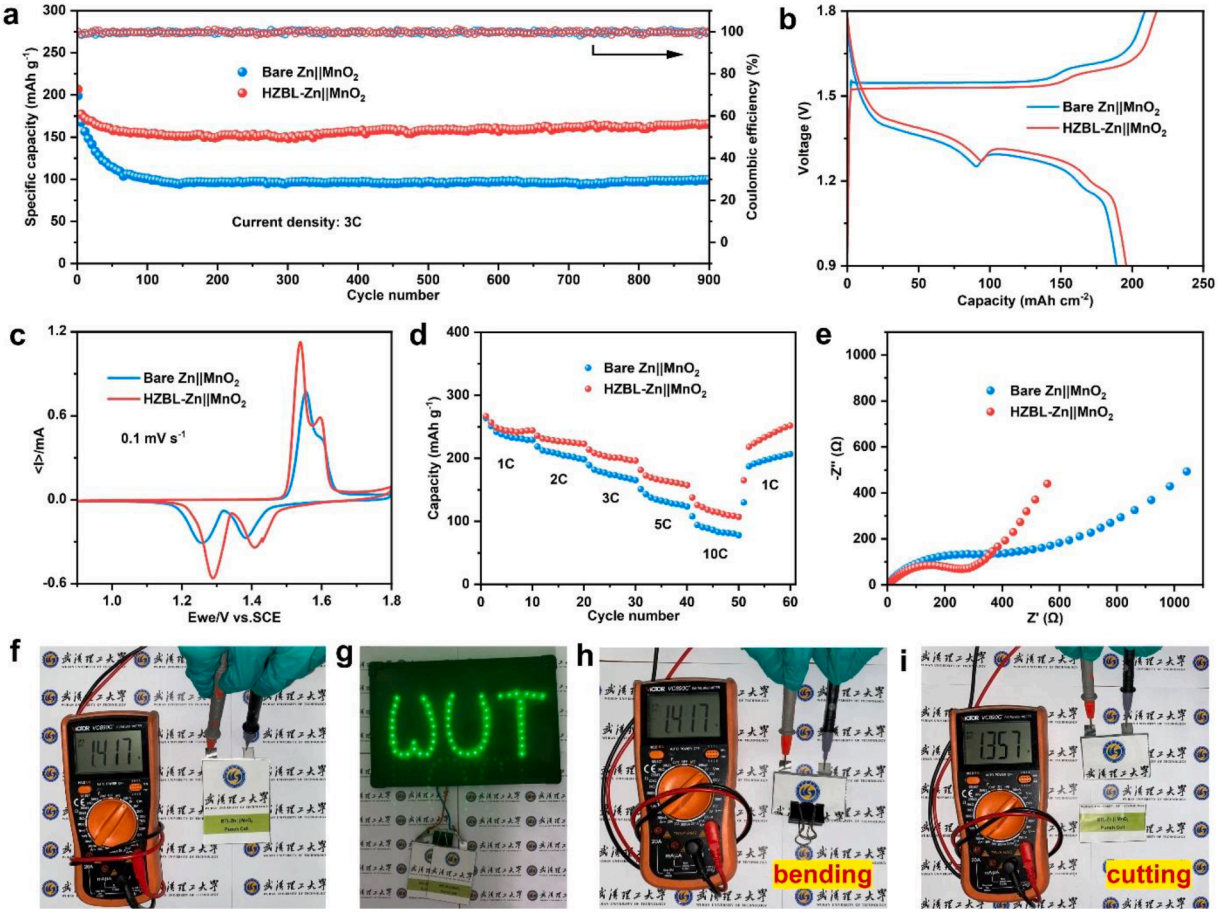

Fig. 6. Electrochemical performance of full cells with HZBL-Zn. a) CE and specific discharge capacity of full cells with bare Zn and HZBL-Zn at 3 C and their b) GCD curves. c) Corresponding CV profiles of full cells. d) Rate performance and e) EIS results of full cell with bare Zn and HZBL-Zn. Digital photos of f) OCV of a punch cell with HZBL-Zn, g) bright LEDs powered by a couple of in series punch cells, OCV of the punch after being h) bent and i) cut.

Conclusion

To sum up, we have designed a novel HZBL on the surface of Zn anodes to realize highly stable anodes in AZBs. Through the reorganization of functional groups, the as-prepared HZBL provides hydrophobic and uniform pathways for zinc ions. On the one hand, hydrophobic skeleton only allow zinc ions to pass through, which can effectively inhibit the HER by prohibiting Zn metal from directly connecting with electrolyte. On the other hand, a succession of zincophilic −COOH groups on sidechains have strong interaction with zinc ions, which can propel the transport of zinc ions and restrict its deposition to ameliorate dendrite growth. As a result, the symmetrical cells with HZBL-Zn prolong the lifespan to 2700 h at a current density of 1 mA cm^{-2}. Moreover, Zn||HZBL-Cu delivers an ultrahigh average CE of 99.88% after 2700 cycles, which is 15 times longer than Zn||bare Cu. Importantly, the superiority of coated Zn in practical application is also confirmed in full batteries coupled with MnO_2. Compared with bare Zn||MnO_2, the full cell with HZBL-Zn produces a higher capacity retention of 80.4% after 900 cycles at 3 C. This unique design of HZBL is expected to open up a bright avenue for the development of high-performance metal anodes in aqueous rechargeable batteries.

CRediT authorship contribution statement

Xuan Zhou: Conceptualization, Methodology, Investigation, Data curation, Visualization, Writing – original draft, Writing – review & editing. **Renpeng Chen:** Conceptualization, Methodology, Data curation, Writing – review & editing. **Enhui Cui:** Conceptualization, Methodology. **Qin Liu:** Writing – review & editing. **Hong Zhang:** Methodology, Data curation. **Jiahui Deng:** Writing – review & editing. **Nannan Zhang:** Writing – review & editing. **Can Xie:** Writing – review & editing. **Lin Xu:** Conceptualization, Writing – review & editing, Supervision, Funding acquisition, Project administration, Resources. **Liqiang Mai:** Funding acquisition, Project administration, Resources.

Declaration of Competing Interest

The authors declare no conflict of interest.

Acknowledgements

This work was supported by the National Natural Science Foundation of China (52272234, 51832004), the National Key Research and Development Program of China (2020YFA0715000), the Key Research and Development Program of Hubei Province (2021BAA070), Independent Innovation Projects of the Hubei Longzhong Laboratory (2022ZZ-20), the Sanya Science and Education Innovation Park of Wuhan University of Technology (2021KF0011).

Supplementary materials

Supplementary material associated with this article can be found, in the online version, at doi:10.1016/j.ensm.2022.12.019.

References

[1] A. Sumboja, B. Prakoso, Y. Ma, F.R. Irwan, J.J. Hutani, A. Mulyadewi, M.A. A. Mahbub, Y. Zong, Z. Liu, FeCo Nanoparticle-Loaded Nutshell-Derived Porous Carbon as Sustainable Catalyst in Al-Air Batteries, Energy Mater. Adv. 2021 (2021) 1–12.

[2] X. Yuan, F. Ma, L. Zuo, J. Wang, N. Yu, Y. Chen, Y. Zhu, Q. Huang, R. Holze, Y. Wu, T. van Ree, Latest Advances in High-Voltage and High-Energy-Density Aqueous Rechargeable Batteries, Electrochem. Energy Rev. 4 (2020) 1–34.

[3] P. Yu, Y. Zeng, H. Zhang, M. Yu, Y. Tong, X. Lu, Flexible Zn-Ion Batteries: Recent Progresses and Challenges, Small 15 (2019), 1804760.

[4] H. Jia, Z. Wang, B. Tawiah, Y. Wang, C.-Y. Chan, B. Fei, F. Pan, Recent advances in zinc anodes for high-performance aqueous Zn-ion batteries, Nano Energy 70 (2020), 104523.

[5] M. Wang, Y. Meng, K. Li, T. Ahmad, N. Chen, Y. Xu, J. Sun, M. Chuai, X. Zheng, Y. Yuan, C. Shen, Z. Zhang, W. Chen, Toward dendrite-free and anti-corrosion Zn anodes by regulating a bismuth-based energizer, eScience 2 (2022) 509–517.

[6] T. Zhang, Y. Tang, S. Guo, X. Cao, A. Pan, G. Fang, J. Zhou, S. Liang, Fundamentals and perspectives in developing zinc-ion battery electrolytes: a comprehensive review, Energy Environ. Sci. 13 (2020) 4625–4665.

[7] L.E. Blanc, D. Kundu, L.F. Nazar, Scientific Challenges for the Implementation of Zn-Ion Batteries, Joule 4 (2020) 771–799.

[8] X. Wu, Y. Xu, C. Zhang, D.P. Leonard, A. Markir, J. Lu, X. Ji, Reverse Dual-Ion Battery via a $ZnCl_2$ Water-in-Salt Electrolyte, J. Am. Chem. Soc. 141 (2019) 6338–6344.

[9] M. Nakamura, N. Sato, N. Hoshi, O. Sakata, Outer Helmholtz plane of the electrical double layer formed at the solid electrode-liquid interface, Chemphyschem 12 (2011) 1430–1434.

[10] N. Wang, H. Wan, J. Duan, X. Wang, L. Tao, J. Zhang, H. Wang, A review of zinc-based battery from alkaline to acid, Mater. Today Adv. 11 (2021), 100149.

[11] F. Wang, O. Borodin, T. Gao, X. Fan, W. Sun, F. Han, A. Faraone, J.A. Dura, K. Xu, C. Wang, Highly reversible zinc metal anode for aqueous batteries, Nat. Mater. 17 (2018) 543–549.

[12] R. Chen, Q. Liu, L. Xu, X. Zuo, F. Liu, J. Zhang, X. Zhou, L. Mai, Zwitterionic Bifunctional Layer for Reversible Zn Anode, ACS Energy Lett 7 (2022) 1719–1727.

[13] B. Sun, P. Xiong, U. Maitra, D. Langsdorf, K. Yan, C. Wang, J. Janek, D. Schroder, G. Wang, Design Strategies to Enable the Efficient Use of Sodium Metal Anodes in High-Energy Batteries, Adv. Mater. 32 (2020), 1903891.

[14] Y. Tian, Y. An, C. Wei, B. Xi, S. Xiong, J. Feng, Y. Qian, Flexible and Free-Standing $Ti_3C_2T_x$ MXene@Zn Paper for Dendrite-Free Aqueous Zinc Metal Batteries and Nonaqueous Lithium Metal Batteries, ACS Nano 13 (2019) 11676–11685.

[15] Z. Hong, Z. Ahmad, V. Viswanathan, Design Principles for Dendrite Suppression with Porous Polymer/Aqueous Solution Hybrid Electrolyte for Zn Metal Anodes, ACS Energy Lett 5 (2020) 2466–2474.

[16] Q. Yang, G. Liang, Y. Guo, Z. Liu, B. Yan, D. Wang, Z. Huang, X. Li, J. Fan, C. Zhi, Do Zinc Dendrites Exist in Neutral Zinc Batteries: A Developed Electrohealing Strategy to In Situ Rescue In-Service Batteries, Adv. Mater. 31 (2019), 1903778.

[17] Z. Cai, Y. Ou, J. Wang, R. Xiao, L. Fu, Z. Yuan, R. Zhan, Y. Sun, Chemically resistant Cu–Zn/Zn composite anode for long cycling aqueous batteries, Energy Storage Mater 27 (2020) 205–211.

[18] C. Li, X. Shi, S. Liang, X. Ma, M. Han, X. Wu, J. Zhou, Spatially homogeneous copper foam as surface dendrite-free host for zinc metal anode, Chem. Eng. J. 379 (2020), 122248.

[19] L. Dong, W. Yang, W. Yang, H. Tian, Y. Huang, X. Wang, C. Xu, C. Wang, F. Kang, G. Wang, Flexible and conductive scaffold-stabilized zinc metal anodes for ultralong-life zinc-ion batteries and zinc-ion hybrid capacitors, Chem. Eng. J. 384 (2020), 123355.

[20] Y. Zhou, X. Wang, X. Shen, Y. Shi, C. Zhu, S. Zeng, H. Xu, P. Cao, Y. Wang, J. Di, Q. Li, 3D confined zinc plating/stripping with high discharge depth and excellent high-rate reversibility, J. Mater. Chem. A 8 (2020) 11719–11727.

[21] H. Yang, Z. Chang, Y. Qiao, H. Deng, X. Mu, P. He, H. Zhou, Constructing a Super-Saturated Electrolyte Front Surface for Stable Rechargeable Aqueous Zinc Batteries, Angew. Chem., Int. Ed. 59 (2020) 9377–9381.

[22] R. Yuksel, O. Buyukcakir, W.K. Seong, R.S. Ruoff, Metal-Organic Framework Integrated Anodes for Aqueous Zinc-Ion Batteries, Adv. Energy Mater. 10 (2020), 1904215.

[23] S.B. Wang, Q. Ran, R.Q. Yao, H. Shi, Z. Wen, M. Zhao, X.Y. Lang, Q. Jiang, Lamella-nanostructured eutectic zinc-aluminum alloys as reversible and dendrite-free anodes for aqueous rechargeable batteries, Nat. Commun. 11 (2020) 1634.

[24] Z. Wang, J. Huang, Z. Guo, X. Dong, Y. Liu, Y. Wang, Y. Xia, A Metal-Organic Framework Host for Highly Reversible Dendrite-free Zinc Metal Anodes, Joule 3 (2019) 1289–1300.

[25] C.Y. Chen, K. Matsumoto, K. Kubota, R. Hagiwara, Q. Xu, A Room-Temperature Molten Hydrate Electrolyte for Rechargeable Zinc-Air Batteries, Adv. Energy Mater. 9 (2019), 1900196.

[26] L. Wang, Y. Zhang, H. Hu, H.Y. Shi, Y. Song, D. Guo, X.X. Liu, X. Sun, A $Zn(ClO_4)_2$ Electrolyte Enabling Long-Life Zinc Metal Electrodes for Rechargeable Aqueous Zinc Batteries, ACS Appl. Mater. Interfaces 11 (2019) 42000–42005.

[27] L. Ma, S. Chen, N. Li, Z. Liu, Z. Tang, J.A. Zapien, S. Chen, J. Fan, C. Zhi, Hydrogen-Free and Dendrite-Free All-Solid-State Zn-Ion Batteries, Adv. Mater. 32 (2020), 1908121.

[28] Y. Zhang, G. Wan, N.H.C. Lewis, J. Mars, S.E. Bone, H.-G. Steinrück, M. R. Lukatskaya, N.J. Weadock, M. Bajdich, O. Borodin, A. Tokmakoff, M.F. Toney, E. J. Maginn, Water or Anion? Uncovering the Zn^{2+} Solvation Environment in Mixed $Zn(TFSI)_2$ and LiTFSI Water-in-Salt Electrolytes, ACS Energy Lett. 6 (2021) 3458–3463.

[29] M. Yan, N. Dong, X. Zhao, Y. Sun, H. Pan, Tailoring the Stability and Kinetics of Zn Anodes through Trace Organic Polymer Additives in Dilute Aqueous Electrolyte, ACS Energy Lett 6 (2021) 3236–3243.

[30] Q. Zhang, J. Luan, L. Fu, S. Wu, Y. Tang, X. Ji, H. Wang, The Three-Dimensional Dendrite-Free Zinc Anode on a Copper Mesh with a Zinc-Oriented Polyacrylamide Electrolyte Additive, Angew. Chem. Int. Ed. 58 (2019) 15841–15847.

[31] Y. Qin, H. Li, C. Han, F. Mo, X. Wang, Chemical Welding of Electrode-Electrolyte Interface by Zn Metal-Initiated in-situ Gelation for Ultralong-Life Zn-Ion Batteries, Adv. Mater. 34 (2022), 2207118.

[32] J.L. Yang, J. Li, J.W. Zhao, K. Liu, P. Yang, H.J. Fan, Stable Zinc Anodes Enabled by a Zincophilic Polyanionic Hydrogel Layer, Adv. Mater. 34 (2022), 2202382.

[33] Q. Liu, Y. Wang, X. Hong, R. Zhou, Z. Hou, B. Zhang, Elastomer–Alginate Interface for High-Power and High-Energy Zn Metal Anodes, Adv. Energy Mater. 12 (2022), 2200318.

[34] Z. Tao, Y. Zhu, Z. Zhou, A. Wang, Y. Tan, Z. Chen, M. Yu, Y. Yang, Constructing Hydrophobic Interface with Close-Packed Coordination Supramolecular Network for Long-Cycling and Dendrite-Free Zn-Metal Batteries, Small 18 (2022), 2107971.

[35] P. Chen, X. Yuan, Y. Xia, Y. Zhang, L. Fu, L. Liu, N. Yu, Q. Huang, B. Wang, X. Hu, Y. Wu, T. van Ree, An Artificial Polyacrylonitrile Coating Layer Confining Zinc Dendrite Growth for Highly Reversible Aqueous Zinc-Based Batteries, Adv. Sci. 8 (2021), 2100309.

[36] N. Zhang, S. Huang, Z. Yuan, J. Zhu, Z. Zhao, Z. Niu, Direct Self-Assembly of MXene on Zn Anodes for Dendrite-Free Aqueous Zinc-Ion Batteries, Angew. Chem., Int. Ed. 60 (2021) 2861–2865.

[37] Q. Zhang, J. Luan, X. Huang, Q. Wang, D. Sun, Y. Tang, X. Ji, H. Wang, Revealing the role of crystal orientation of protective layers for stable zinc anode, Nat. Commun. 11 (2020) 3961.

[38] R. Zhao, Y. Yang, G. Liu, R. Zhu, J. Huang, Z. Chen, Z. Gao, X. Chen, L. Qie, Redirected Zn Electrodeposition by an Anti-Corrosion Elastic Constraint for Highly Reversible Zn Anodes, Adv. Funct. Mater. 31 (2020), 2001867.

[39] H. He, H. Tong, X. Song, X. Song, J. Liu, Highly stable Zn metal anodes enabled by atomic layer deposited Al_2O_3 coating for aqueous zinc-ion batteries, J. Mater. Chem. A 8 (2020) 7836–7846.

[40] Y. Cui, Q. Zhao, X. Wu, X. Chen, J. Yang, Y. Wang, R. Qin, S. Ding, Y. Song, J. Wu, K. Yang, Z. Wang, Z. Mei, Z. Song, H. Wu, Z. Jiang, G. Qian, L. Yang, F. Pan, An Interface-Bridged Organic-Inorganic Layer that Suppresses Dendrite Formation and Side Reactions for Ultra-Long-Life Aqueous Zinc Metal Anodes, Angew. Chem. Int. Ed. 59 (2020) 16594–16601.

[41] B.P. Rocky, A.J. Thompson, Analyses of the Chemical Compositions and Structures of Four Bamboo Species and their Natural Fibers by Infrared, Laser, and X-ray Spectroscopies, Fiber. Polym. 22 (2021) 916–927.

[42] D. Xiaodong, Y. Shuanglin, Y. Yuan, L. Huanrong, N, O, and S functional groups in residue asphaltene before and after hydrotreating via X-ray technology, Petrol. Sci. Technol. 35 (2017) 988–992.

[43] B. Li, T. He, Z. Wang, Z. Cheng, Y. Liu, T. Chen, W. Lai, X. Wang, X. Liu, Chemical reactivity of C-F bonds attached to graphene with diamines depending on their nature and location, Phys. Chem. Chem. Phys. 18 (2016) 17495–17505.

[44] M.R. Lacroix, Y. Liu, S.H. Strauss, Room-Temperature FTIR Spectra of the Cyclic $S_4(H_2O)_4$ Cluster in Crystalline $Li_2(H_2O)_4(B_{12}F_{12})$: Observation of B and E nu(OH) Bands and Coupling of Strong O-H...O and Weak O-H...F Vibrations, J. Phys. Chem. A 123 (2019) 9781–9790.

[45] X. Nie, F. Dong, M. Liu, W. Cheng, C. Ding, L. Bian, S. Sun, Bonding Behavior and Mechanism of U(VI) by Chemically Modified Deinococcus radiodurans, Minerals 11 (2021) 1108.

[46] Z. Zhao, J. Zhao, Z. Hu, J. Li, J. Li, Y. Zhang, C. Wang, G. Cui, Long-life and deeply rechargeable aqueous Zn anodes enabled by a multifunctional brightener-inspired interphase, Energy Environ. Sci. 12 (2019) 1938–1949.

[47] M. Abdallah, Ethoxylated fatty alcohols as corrosion inhibitors for dissolution of zinc in hydrochloric acid, Corros. Sci. 45 (2003) 2705–2716.

[48] G. Trejo, H. Ruiz, R. Borges, Y. Meas, Influence of polyethoxylated additives on zinc electrodeposition from acidic solutions, J. Appl. Electrochem. 31 (2001) 685–692.

[49] J.C. Ballesteros, P. Díaz-Arista, Y. Meas, R. Ortega, G. Trejo, Zinc electrodeposition in the presence of polyethylene glycol 20000, Electrochim. Acta 52 (2007) 3686–3696.

[50] P. Cao, X. Zhou, A. Wei, Q. Meng, H. Ye, W. Liu, J. Tang, J. Yang, Fast-Charging and Ultrahigh-Capacity Zinc Metal Anode for High-Performance Aqueous Zinc-Ion Batteries, Adv. Funct. Mater. 31 (2021), 2100398.

[51] Z. Hou, Y. Gao, R. Zhou, B. Zhang, Unraveling the Rate-Dependent Stability of Metal Anodes and Its Implication in Designing Cycling Protocol, Adv. Funct. Mater. 32 (2021), 2107584.

[52] J. Hao, T. Meng, D. Shu, X. Song, H. Cheng, B. Li, X. Zhou, F. Zhang, Z. Li, C. He, Synthesis of three dimensional N&S co-doped rGO foam with high capacity and long cycling stability for supercapacitors, J. Colloid Interface Sci. 537 (2019) 57–65.